Nanoscale Advances

ROYAL SOCIETY OF CHEMISTRY

COMMUNICATION

View Article Online
View Journal | View Issue

Cite this: *Nanoscale Adv.*, 2023, **5**, 1624

Improved photovoltaic performance of Pb-free $AgBi_2I_7$ based photovoltaics†

Praveen Kumar,[a] Khursheed Ahmad[a] and Shaikh M. Mobin *[abc]

Received 13th January 2023
Accepted 9th February 2023

DOI: 10.1039/d3na00029j

rsc.li/nanoscale-advances

Hybrid perovskites based on bismuth are good candidates for developing lead-free and air-stable photovoltaics, but they have historically been constrained by poor surface morphologies and large band-gap energies. Monovalent silver cations are incorporated into iodobismuthates as part of a novel materials processing method to fabricate improved bismuth-based thin-film photovoltaic absorbers. However, a number of fundamental characteristics prevented them from achieving better efficiency. We examine bismuth iodide perovskite made of silver with improvements in surface morphology and a narrow band gap, and we achieve high power conversion efficiency. $AgBi_2I_7$ perovskite was used in the fabrication of PSCs as a material for light absorption, and its optoelectronic proficiencies were also studied. We reduced the band gap to 1.89 eV and achieved a maximum power conversion efficiency of 0.96% using the solvent engineering approach. Additionally, simulation studies verified an efficiency of 13.26% by using $AgBi_2I_7$ as a light absorber perovskite material.

Due to their exceptional semiconducting characteristics, such as relatively low carrier recombination rates,[1,2] long carrier diffusion lengths,[2] low charge carrier mobilities,[3,4] stoichiometry-tunable band gaps,[5,6] and high absorption coefficients, lead-based halide perovskites have recently attracted a lot of attention.[7] Formamidinium lead iodide ($FAPbI_3$), one of the perovskite systems, has drawn the most interest because of its outstanding performance in thin-film solar cells, where it can achieve a power conversion efficiency (PCE) of 25.7%.[8] However, the presence of noxious Pb and the product's fragility when exposed to moisture and temperature have led to grave worries about its viability for commercial use. There has been a lot of interest in developing halide perovskite solar cells that are non or low-toxic and air stable. As a result, efforts have been made to develop perovskite solar cells and seek alternatives to lead. Many perovskites based on tin (Sn)[9] and germanium (Ge)[10] have been investigated to address the issue of toxicity. Song *et al.*[11] designed and manufactured Sn-based perovskite materials containing caesium (Cs) as a cation, with $CsSnI_3$ and $CsSnBr_3$ perovskites achieving efficiencies of 3.04% and 1.83%, respectively. In addition, Ke *et al.*[12] used a unique hollow 3-D perovskite [$enFASnI_3$] as a light absorber material in perovskite solar cells (PSCs), with a 7.1% efficiency. Mhaisalkar and colleagues used a Ge-based $AGeI_3$ perovskite-like material.[13] These Sn and Ge based perovskite-like materials have a high efficiency, but they must be handled with caution since they are air sensitive and need an inert environment to be stable. The perovskite structure is distorted by the quick shift in the oxidation states of Sn and Ge by +2. Moreover, when compared to Pb, these Sn and Ge based perovskites are unable to reach high efficiency. However, instability and poor performance of Sn and Ge based devices under ambient conditions owing to disproportionation are disappointing.

There have been several reports on the use of copper (Cu) as a metal ion in PSCs, utilising a lead-free approach. Mathews *et al.*,[14] Ahmad *et al.*,[15] and Li *et al.*[16] utilized $MA_2CuCl_xBr_{4-x}$ and $C_6H_4NH_2CuBr_2I$ perovskite materials as light absorbers in photovoltaic applications. Although these Cu-based perovskites have high stability, they are inefficient in producing good PCE. Yang *et al.*,[17] Wang *et al.*,[18] and Vargas *et al.*[19] studied the optoelectronic activity of $(C_6H_5CH_2NH_3)_2CuBr_4$, $(H_3NC_6H_4NH_3)CuBr_4$, and $Cs_4CuSb_2Cl_{12}$ perovskite materials, respectively. Further, lead(II), bismuth (Bi^{3+}), and antimony (Sb^{3+}) ions are isoelectronic ($6s^2$), and they may be stable and safe substitutes in thin-film photovoltaic (PV) systems. Bi^{3+} may be used to manufacture PSCs as a non-toxic metal ion, which is promising for replacing Pb and Sn metals. The $A_3Bi_2I_9$ basic formula (A = Cs^+, MA^+, NH_4^+, B = Bi^{3+}, Sb^{3+}, X = Cl^-, Br^-, I^-) has been widely employed in the design and manufacture of lead-free perovskite solar cells. Mobin *et al.*[20] created $Cs_3Sb_2I_9$ and $Cs_3Bi_2I_9$

[a]*Department of Chemistry, Indian Institute of Technology Indore, Simrol, Khandwa Road, Indore 453552, India. E-mail: xray@iiti.ac.in*

[b]*Department of Biosciences and Bio-Medical Engineering, Indian Institute of Technology Indore, Simrol, Khandwa Road, Indore 453552, India*

[c]*Center for Advanced Electronics (CAE), Indian Institute of Technology Indore, Simrol, Khandwa Road, Indore 453552, India*

† Electronic supplementary information (ESI) available. See DOI: https://doi.org/10.1039/d3na00029j

perovskites with a PCE of above 1%. Hebig *et al.*[21] and Ahmad *et al.*[22] used $MA_3Sb_2I_9$ for photovoltaic applications, whereas Kumar *et al.*[23] and Zuo *et al.*[24] used $(NH_4)_3Sb_2I_9$ perovskite as the light absorber and developed a device that demonstrated the potential of Bi^{3+} in PSCs. Okano *et al.*[25] and Ahmad *et al.*[26] employed a gas-assisted and two-step manufacturing technique to prepare $(CH_3NH_3)_3Bi_2I_9$ for PSCs, respectively. Kulkarni *et al.*[27] used an *N*-methyl pyrrolidone-assisted method and achieved 0.31% PCE. Huang *et al.*[28] obtained 0.06% PCE using fluorinated perylene diimide (FPDI) as an ETL (electron transport layer) in the $(CH_3NH_3)_3Bi_2I_9$ PSC. This low PCE might be due to the FPDI's weak surface or charge extraction issue. Sun *et al.*[29] and Zhuang *et al.*,[30] on the other hand, looked into the crystalline properties of $(NH_4)_3Bi_2I_9$ perovskite and used it in X-rays and PSCs, respectively. Furthermore, their broad band gap and low PCE reduce the likelihood of commercialization. To improve photovoltaic efficiency, 3D structures based on silver-bismuth iodide are used. Filip *et al.* suggested double halide perovskites like $Cs_2BiAgCl_6$ and $Cs_2BiAgBr_6$ in 2016.[31] $AgBi_2I_7$ perovskite has recently attracted interest because of its efficiency and narrow band gap (<2.0 eV), which improve light harvesting characteristics. Kim *et al.*[32] reported the first Ag-based PSC using Bi as the metal ion in 2016 and attained a PCE of 1.2%. However, when Shao *et al.*[33,34] and Johansson *et al.*[35] employed the same methodology, the performance of $AgBi_2I_7$ perovskite changed with photovoltaic efficiency. Reproducing the solar cell yielded just 0.52 and 0.4% efficiency.[33–35] $AgBi_2I_7$ perovskite's sensitivity can make up for its lack of repeatability, or it could be caused by the annealing temperature. To comprehend and modify the attributes of Ag-based Bi PSCs, we synthesised $AgBi_2I_7$ (SBI).

We have studied the solution engineering approach to improve the photovoltaic performance of silver-based bismuth iodide perovskites as light absorbers. To our knowledge, this is the first report on the use of SBI perovskites as light absorbers in the presence of DMF and DMF : MeOH. The impact of the solvent engineering strategy on the fabrication of SBI perovskite solar cells may be immediately seen in their efficiency and photovoltaic properties. In the present work, we employed DMF and MeOH, two different solvents in an appropriate ratio, and with molar ratio 1 : 2 of AgI and BiI_3 respectively. $AgBi_2I_7$ DMF (SBI-D) and $AgBi_2I_7$ DMF : MeOH (SBI-DM) were spin coated onto the conductive glass electrode (FTO) at 1500 rpm for 30 seconds (Scheme 1). Other fabrication data are provided in the ESI.† A convincing demonstration of the equimolar ratio of both the solvent (DMF : MeOH) gives the highest PCE as compared to only 0.96% with DMF under 1 sun illumination conditions and 30–40% humidity.

PXRD was used to characterise the phase purity and formation of the SBI perovskite material synthesized with both DMF and DMF : MeOH solvents, with the findings shown in Fig. 1A. The formation and crystalline nature of SBI-D (DMF : MeOH = 1 : 0) and SBI-DM (DMF : MeOH = 0.5 : 0.5) perovskite materials were revealed by PXRD peak patterns. The growth of SBI-D and SBI-DM is supported by the appearance of a prominent diffraction peak in the (333) plane.

The stability of perovskite may be assessed using the Goldschmidt tolerance factor (t); when the value of "t" is between 0.8 and 1, it implies that the perovskite structure is stable.[36] Another important component in the cubic crystal is the ionic radius of A, which should not be either large (then, $t > 1$) or too small (then, $t < 0.8$) in comparison to the ionic radius of B. If the ionic radius of A is substantially bigger than that of B, it will not fit inside the BX_8 octahedron. This could originate from a distinct perovskite structure. The tolerance factor and octahedron ratio are described by eqn (a) and (b):

$$(t) = \frac{(r_A + r_X)}{\sqrt{2}(r_B + r_X)} \quad \text{(a)}$$

$$(\mu) = \frac{r_B}{r_X} \quad \text{(b)}$$

where r_A, r_B, and r_X stand for ionic radii of A, B, and X present in the perovskite (ABX_3) structure.

At $t = 1$, the predicted perfect cubic structure was seen. In order to produce a stable octahedron for a cubic cell, the octahedron factor (μ) should be between 0.44 and 0.72. The effective ionic radii of silver (Ag) and bismuth (Bi) are 1.26 Å and 1.03 Å, respectively, which are appropriate for the creation of a stable cubic perovskite structure. We may infer and remark on the stability of our perovskite based on this finding, and therefore, it can also be employed as a light absorber material in photovoltaic applications.

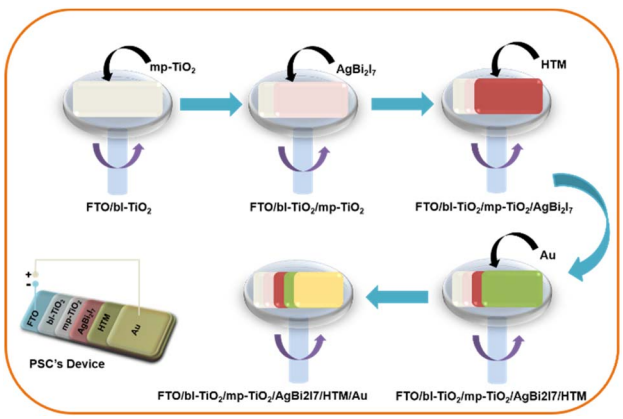

Scheme 1 Schematic of the fabrication procedure of the perovskite solar cell.

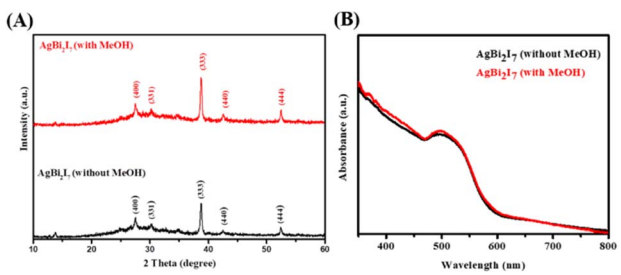

Fig. 1 PXRD peak pattern (A) and UV-vis absorption spectra (B) of $AgBi_2I_7$ perovskite with MeOH (red) and without MeOH (black).

UV/vis spectroscopy was used to determine the optical characteristics of SBI-D and SBI-DM thin films (Fig. 1B). The absorption spectra of these perovskite materials were nearly identical. The optical band gaps for SBI-D and SBI-DM may be calculated using UV absorption spectra and linear extrapolation of Tauc plots (Fig. S1†).[37] The optical band gap was calculated to be 1.89 eV using the Tauc plot ($(\alpha h\nu)^n$ against $h\nu$), where α, h and ν are the absorption coefficient, Planck's constant, and excitation frequency respectively. The computed optical band gap reveals that the produced perovskite has high absorbance and has the potential to be used as a light absorber in solar cells.

Surface morphology investigation was done using FE-SEM to evaluate the impact of engagement and solvent content on the perovskite SBI material. The surface morphology of SBI-D and SBI-DM is shown in Fig. 2A–D, and it was obvious that only the DMF solvent produced a rod-like shape, whereas the DMF : MeOH combination produced a distorted rod-like morphology that was converted to a uniform surface morphology.

This might be due to perovskite suppressing and regulating the quick crystallisation process. It has been discovered that a pinhole-free, smooth layer can improve the photovoltaic efficiency of perovskite solar cells.

When a photon strikes a perovskite material, it generates an electron and hole pair. The produced electron was excited and moved towards the LUMO (lowest unoccupied molecular orbital) level, from where it was transferred to conductive glass (FTO) through mesoporous-TiO_2 and blocking-TiO_2 LUMO levels. The produced electrons are contained in FTO glass, while the remaining hole in the perovskite material is carried *via* the HTM (hole transport material) to complete the circuit. Scheme 2 explains the entire electron transfer mechanism in simple terms. All of the energy levels of the conductive glass, ETL, and HTM, such as bl-TiO_2, mp-TiO_2, Spiro-MeOTAD, and Au, have been extracted from previously published literature. In addition, using UV-visible and cyclic voltammetry (CV) techniques, the HOMO–LUMO energy levels of our perovskite materials SBI were estimated similarly to previous reports.

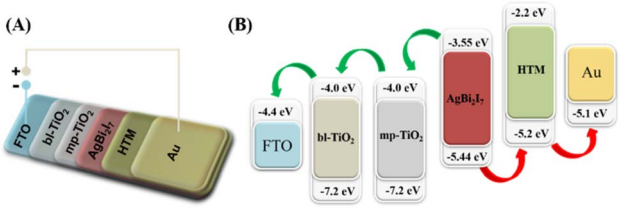

Scheme 2 Schematic device structure (A) and materials energy level diagram (B) of the SBI based PSCs. Energy level values as per reported literature.

The optical band gap of SBI was determined using a Tauc plot, whereas the onset reduction potential (E_{red}) was determined using a CV graph (Fig. S2†). We determine the energy levels of the SBI perovskite material using eqn (i) and (ii).[38] All of the CV measurement details are included in the ESI.†

$$E_{CB}\ (E_{LUMO}) = -(E_{red} + 4.725)\ \text{eV} \quad \text{(i)}$$

$$E_{VB}\ (E_{HOMO}) = -(E_{CB} - E_g)\ \text{eV} \quad \text{(ii)}$$

Here, E_g and E_{red} stand for the optical band gap and onset reduction potential, and E_{CB} and E_{VB} are conduction and valence band energy levels.

Henceforth, we compared our computed SBI perovskite energy levels (E_{CB} and E_{VB}) to the ETL and HTM for smooth charge transfer. The results indicate an excellent correlation between the HOMO and LUMO levels, implying that SBI perovskite has potential as a light absorber material.

Moreover, a PSC device was designed using $AgBi_2I_7$ as a perovskite light absorber; comprehensive device fabrication details are included in the ESI†. The device's photovoltaic performance was measured after it was fabricated under ambient conditions (30–40% humidity). The short circuit photocurrent density–voltage curve was used to assess the device's photovoltaic performance. Fig. 3 shows the photovoltaic performance of SBI-D and SBI-DM under one sun conditions (1.5 AM; 100 mW cm^{-2}). Table 1 contains all of the photovoltaic parameters recorded by the devices. The maximum PCE of 0.96% was reached using SBI-DM PSCs, which is higher

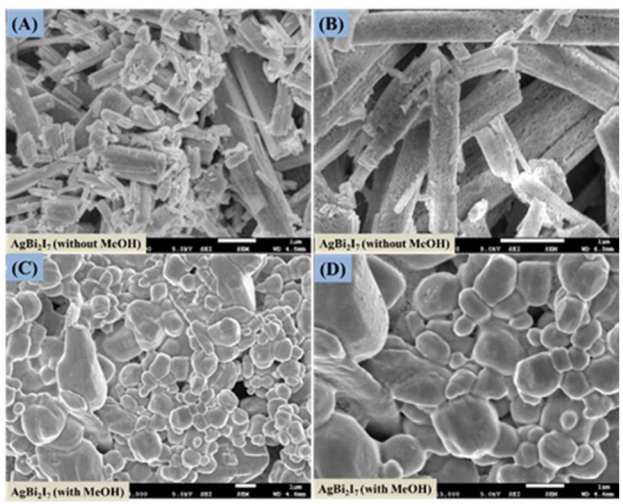

Fig. 2 FE-scanning electron microscopy images of $AgBi_2I_7$ perovskite without MeOH (A and B) and with MeOH (C and D).

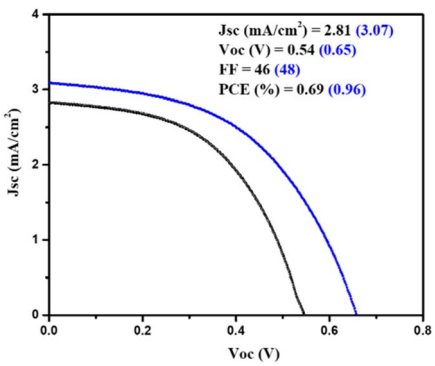

Fig. 3 Showing the photovoltaic performance of SBI-D and SBI-DM under 1 sun conditions.

Table 1 Showing the comparison of reported photovoltaic performances with SBI-D and SBI-DM

Light absorbers	V_{oc} (mV)	FF (%)	J_{sc} (mA cm^{-2})	PCE (%)	References
$(CH_3NH_3)_3Sb_2I_9$	896	55	1.0	0.49	21
$C_6H_4NH_2CuBr_2I$	200	46	6.2	0.46	16
Cs_2SnI_6	520	52	3.2	0.86	39
$AgBi_2I_7$	690	43	2.76	0.83	40
$(CH_3NH_3)_3Sb_2I_9$	740	52	1.48	0.57	41
Cs_2NaBiI_6	470	44	1.99	0.42	42
$Cs_3Bi_2I_9$	570	222	49	0.62	43
$(NH_4)_3Sb_2I_9$	1003	115	42.9	0.51	44
$CH_3NH_3SnBr_3$	490	46	2.2	0.5	45
$(MA_3(Bi_{1-x}Sn_x)_2I_9)$	556	48	3.70	0.91	46
SBI-D	540	46	2.81	0.69	**This work**
SBI-DM	650	48	3.07	0.96	

than the PCE of PSCs manufactured with SBI-D as a light absorber. Additionally, Fig. S5, ESI† provides the box charts of the J_{sc}, FF, V_{oc}, and PCE for SBI-D and SBI-DM. Moreover, SBI-DM perovskite as a light absorber attained a higher open circuit voltage than SBI-D PSCs. However, $AgBi_2I_7$ synthesized from DMF and MeOH solutions revealed homogeneous grains and a thin uniform layer, providing an easy interaction with surrounding charge transfer layers. It is observed from the XRD and SEM results that the solvent in the precursor solution significantly affects the crystallization and morphology of $AgBi_2I_7$. This solvent engineering approach showed the improvement in morphology without affecting the perovskite structure, which resulted in an increase in efficiency.

We summarized all data in Table 1 for comparison with other reported photovoltaic performances of Pb free PSCs. Recently, there has been a tremendous increase in the production of Pb-free PSCs. The research and development of non-toxic perovskite materials for photovoltaic applications has garnered considerable interest from researchers. 0-D $(CH_3NH_3)_3Sb_2I_9$ perovskite was introduced by Hebig *et al.*[21] as a potential contender for lead-free perovskite solar cells. Additionally, a PCE of 0.49% was obtained by using solvent engineering techniques that included a toluene drop during the spin-coating procedure. Li *et al.*[16] created a novel form of photovoltaic material with a band gap of 1.64 eV, although they only managed to obtain a 0.46% efficiency. For PSCs, Qiu *et al.*[39] used a Cs_2SnI_6 light absorber, but the manufactured device had a subpar PCE of 0.86%. A thin file of $AgBi_2I_7$ perovskite with a direct band gap of 1.93 eV was designed by Shao *et al.*,[40] although the efficiency was only 0.83%. 2018 had seen the utilization of the $(CH_3NH_3)_3Sb_2I_9$ perovskite material in solar cells by Chatterjee *et al.*,[41] and the manufactured PSC device had the best PCE of 0.57% without any dopant. In earlier research, Zhang *et al.*[42] designed a novel perovskite structure; the light absorber (Cs_2NaBiI_6) had good optoelectronic properties, however its PCE was less than 1%. Very stable Pb free PSCs have also been developed using all inorganic perovskite structures, although only 0.62% efficiency was attained.[43] Zuo *et al.*[44] had used variation in halide ions using iodide and bromide ions, with $(NH_4)_3Sb_2I_9$ having the maximum PCE of 0.5%. However, Yokoyama *et al.*[45] and Ahmad *et al.*[46] respectively designed Sn-based perovskites $(CH_3NH_3SnBr_3)$ and Sn-incorporated materials $(MA_3(Bi_{1-x}Sn_x)_2I_9)$, where the PCE was higher with the doped light absorber $(MA_3(Bi_{1-x}Sn_x)_2I_9)$. When compared to previous reported lead-free perovskite devices, the photovoltaic performance of our SBI-D and SBI-DM based PSC devices was superior.

Research is still underway to develop a high-performance, stable device that can meet all energy demands. In this viewpoint, various attempts such as encapsulation, insertion of metal ions, doping of metal ions, and multistep fabrication were done. Different Pb-free PSCs have been developed and manufactured. We also looked into the electrical and optical properties of perovskite light absorbers and charge transport layers, which are important for improving the efficiency of perovskite solar cells. Computational studies were conducted to determine the influence of ETL, HTM, and perovskite material thickness during solar cell fabrication. Understanding the variable performance characteristics of PSCs (FF, V_{oc}, J_{sc}, PCE) in terms of thickness variation was important. The SCAPS-1D programme was used to simulate the $AgBi_2I_7$ lead-free perovskite.[47]

The *J–V* curve and performance metrics for the FTO (500 nm)/TiO_2 (100 nm)/$AgBi_2I_7$ (varying)/Spiro-MeOTAD (100 nm)/Au device architecture are shown in Fig. 4a and b. According to the numerical simulation, the $AgBi_2I_7$ lead-free perovskite's greatest PCE, with a perovskite layer thickness of 500 nm, was 13.26%. When the perovskite material thickness is extended from 100 nm to 500 nm, the J_{sc} value rises while the V_{oc} value somewhat declines but not enough to have an impact on performance. The outstanding $AgBi_2I_7$ perovskite PCE of 13.26% at optimum 500 nm thickness was employed for simulation purposes (Fig. 4).

ETL and HTM effects on performance had been examined to note the impact of perovskite material thickness. The *J–V* curve of a simulation with increasing TiO_2 thickness is shown in Fig. S3a.† A little drop in J_{sc} was seen when the TiO_2 thickness increased from 100 nm to 500 nm. Additionally, this drop in J_{sc} impacts the device PCE as the TiO_2 thickness increases, with only a minimal impact on V_{oc} and FF (Fig. S3b†). As a consequence, simulation findings show that TiO_2 at a thickness of 100 nm is far more effective than that of the ETL. Fig. S4a†

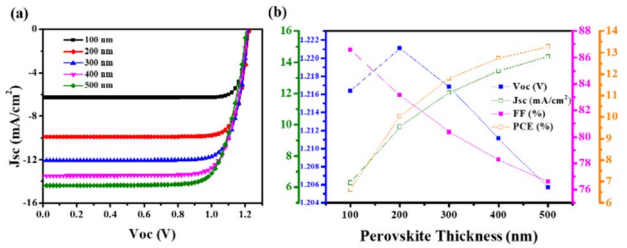

Fig. 4 Photovoltaic performance (*J*–*V*) (a) of the simulated Pb-free PSCs with the device architecture of FTO (500 nm)/TiO_2 (100 nm)/$AgBi_2I_7$ (varying)/Spiro-MeOTAD (100 nm)/Au. Photovoltaic parameters (b) of the simulated Pb-free PSCs with the device architecture of FTO (500 nm)/TiO_2 (100 nm)/$AgBi_2I_7$ (varying)/Spiro-MeOTAD (100 nm)/Au.

shows the *J*–*V* curves of $AgBi_2I_7$ perovskite with various thicknesses of HTMs (Spiro-MeOTAD), which exhibited almost little change in J_{sc} and V_{oc}. The simulated results of the perovskite parameter demonstrate that, with the exception of V_{oc}, all other parameters showed a declining tendency as the thickness of the HTM increased (Fig. S4b†). As a result of its superior performance, modelling of the $AgBi_2I_7$ perovskite was done at a 100 nm TiO_2 and HTM thickness. Recently, computational studies on lead-free perovskite solar cells were also carried out by Mobin *et al.*[46] and relative efficiencies of approximately 12% for the perovskite materials $MA_3(Bi_{1-x}Sn_x)_2I_9$ were reported.

To summarize our conclusions, we used a solvent engineering technique to fabricate a silver based bismuth perovskite ($AgBi_2I_7$) material as a light absorber for PSCs. The photovoltaic efficiency was improved by combining DMF and MeOH in an optimum ratio. The obtained device performance results demonstrate the efficacy of the solvent engineering method. Likewise, using $AgBi_2I_7$ as a light absorber in the device construction of PSCs resulted in a good PCE (0.96%) and V_{oc} (650 mV). In the future perspective, improving system performance may be achieved by comprehending the crystallization process as well as by investigating appropriate charge transport layers and solvents. To improve the optical characteristics of $AgBi_2I_7$, less noxious metals might be inserted or doped into the structure. Additionally, $AgBi_2I_7$ can be applied in different energy-harvesting scenarios.

Conflicts of interest

There are no conflicts to declare.

Acknowledgements

P. K. would like to thank DST-Inspire, New Delhi (India) for the research fellowship. The authors sincerely acknowledge the Department of Chemistry and SIC, IIT Indore for characterization facilities. S. M. M. is thankful to SERB-DST (Project No. CRG/2020/001769), New Delhi, India, BRNS (Project No. 58/14/17/2020-BRNS/37215) and IIT Indore for the financial support and research grant.

References

1 G. Xing, N. Mathews, S. Sun, S. S. Lim, Y. M. Lam, M. Grätzel, S. Mhaisalkar and T. C. Sum, Long-range balanced electron and hole-transport lengths in organic-inorganic $CH_3NH_3PbI_3$, *Science*, 2013, **342**, 344–347.
2 S. D. Stranks, G. E. Eperon, G. Grancini, C. Menelaou, M. J. Alcocer, T. Leijtens, L. M. Herz, A. Petrozza and H. J. Snaith, Electron-hole diffusion lengths exceeding 1 micrometer in an organometal trihalide perovskite absorber, *Science*, 2013, **342**, 341–344.
3 C. S. Ponseca Jr, T. J. Savenije, M. Abdellah, K. Zheng, A. Yartsev, T. Pascher, T. Harlang, P. Chabera, T. Pullerits, A. Stepanov, J.-P. Wolf and V. Sundström, Organometal halide perovskite solar cell materials rationalized: ultrafast charge generation, high and microsecond-long balanced mobilities, and slow recombination, *J. Am. Chem. Soc.*, 2014, **136**, 5189–5192.
4 C. Wehrenfennig, G. E. Eperon, M. B. Johnston, H. J. Snaith and L. M. Herz, High charge carrier mobilities and lifetimes in organolead trihalide perovskites, *Adv. Mater.*, 2014, **26**, 1584–1589.
5 D. P. McMeekin, G. Sadoughi, W. Rehman, G. E. Eperon, M. Saliba, M. T. Hörantner, A. Haghighirad, N. Sakai, L. Korte and B. A. Rech, mixed-cation lead mixed-halide perovskite absorber for tandem solar cells, *Science*, 2016, **351**, 151–155.
6 N. J. Jeon, J. H. Noh, W. S. Yang, Y. C. Kim, S. Ryu, J. Seo and S. I. Seok, Compositional engineering of perovskite materials for high-performance solar cells, *Nature*, 2015, **517**, 476–480.
7 S. D. Wolf, J. Holovsky, S. J. Moon, P. Löper, B. Niesen, M. Ledinsky, F. J. Haug, J. H. Yum and C. Ballif, Organometallic halide perovskites: sharp optical absorption edge and its relation to photovoltaic performance, *J. Phys. Chem. Lett.*, 2014, **5**, 1035–1039.
8 *Research Cell and Champion Module Efficiency Records: National Renewable Energy Laboratory*, **https://www.nrel.gov/pv/cell-efficiency.html**.
9 M. Konstantakou and T. Stergiopoulos, A critical review on tin halide perovskite solar cells, *J. Mater. Chem. A*, 2017, **5**, 11518–11549.
10 I. Kopacic, B. Friesenbichler, S. F. Hoefler, B. Kunert, H. Plank, T. Rath and G. Trimmel, Enhanced Performance of Germanium Halide Perovskite Solar Cells through Compositional Engineering, *ACS Appl. Energy Mater.*, 2018, **1**, 343–347.
11 T.-B. Song, T. Yokoyama, C. C. Stoumpos, J. Logsdon, D. H. Cao, M. R. Wasielewski, S. Aramaki and M. G. Kanatzidis, Importance of reducing vapor atmosphere in the fabrication of tin-based perovskite solar cells, *J. Am. Chem. Soc.*, 2017, **139**, 836–842.
12 W. Ke, C. C. Stoumpos, M. Zhu, L. Mao, I. Spanopoulos, J. Liu, O. Y. Kontsevoi, M. Chen, D. Sarma, Y. Zhang, M. R. Wasielewski and M. G. Kanatzidis, Enhanced photovoltaic performance and stability with a new type of hollow 3D perovskite {en}$FASnI_3$, *Sci. Adv.*, 2017, **3**, 1701293.

13 T. Krishnamoorthy, H. Ding, C. Yan, W. Lin Leong, T. Baikie, Z. Zhang, M. Sherburne, S. Li, M. Asta, N. Mathews and S. G. Mhaisalkar, Lead-free germanium iodide perovskite materials for photovoltaic applications, *J. Mater. Chem. A*, 2015, **3**, 23829–23832.

14 D. Cortecchia, H. A. Dewi, J. Yin, A. Bruno, S. Chen, T. Baikie, P. P. Boix, M. Grätzel, S. Mhaisalkar, C. Soci and N. Mathews, Lead-Free $MA_2CuCl_xBr_{4-x}$ Hybrid Perovskites, *Inorg. Chem.*, 2016, **55**, 1044–1052.

15 K. Ahmad and S. M. Mobin, Organic–Inorganic Copper (II)-Based Perovskites: A Benign Approach toward Low-Toxicity and Water-Stable Light Absorbers for Photovoltaic Applications, *Energy Technol.*, 2020, **8**, 1901185.

16 X. Li, X. Zhong, Y. Hu, B. Li, Y. Sheng, Y. Zhang, C. Weng, M. Feng, H. Han and J. Wang, Organic–inorganic copper (II)-based material: A low-toxic, highly stable light absorber for photovoltaic application, *J. Phys. Chem. Lett.*, 2017, **8**, 1804–1809.

17 X.-L. Li, Z. Li, G. Zhang and G.-J. Yang, Lead-free perovskite $[H_3NC_6H_4NH_3]CuBr_4$ with both a bandgap of 1.43 eV and excellent stability, *J. Mater. Chem. A*, 2020, **8**, 5484–5488.

18 X. Li, B. Li, J. Chang, B. Ding, S. Zheng, Y. Wu, J. Yang, G. Yang, X. Zhong and J. Wang, $(C_6H_5CH_2NH_3)_2CuBr_4$: A Lead-Free, Highly Stable Two-Dimensional Perovskite for Solar Cell Applications, *ACS Appl. Energy Mater.*, 2018, **1**, 2709–2716.

19 B. Vargas, E. Ramos, E. Perez-Gutierrez, J. C. Alonso and D. Solis-Ibarra, A direct bandgap copper–antimony halide perovskite, *J. Am. Chem. Soc.*, 2017, **139**, 9116–9119.

20 K. Ahmad, P. Kumar and S. M. Mobin, Inorganic Pb-Free Perovskite Light Absorbers for Efficient Perovskite Solar Cells with Enhanced Performance, *Chem.–Asian J.*, 2020, **15**, 2859–2863.

21 J. C. Hebig, I. Kühn, J. Flohre and T. Kirchartz, Optoelectronic Properties of $(CH_3NH_3)_3Sb_2I_9$ Thin Films for Photovoltaic Applications, *ACS Energy Lett.*, 2016, **1**, 309–314.

22 K. Ahmad, P. Kumar and S. M. Mobin, A Two-Step Modified Sequential Deposition Method-based Pb-Free $(CH_3NH_3)_3Sb_2I_9$ Perovskite with Improved Open Circuit Voltage and Performance, *ChemElectroChem*, 2020, **7**, 946–950.

23 P. Kumar, K. Ahmad, J. Dagar, E. Unger and S. M. Mobin, Two-Step Deposition Approach for Lead Free $(NH_4)_3Sb_2I_9$ Perovskite Solar Cells with Enhanced Open Circuit Voltage and Performance, *ChemElectroChem*, 2021, **8**, 3150–3154.

24 C. Zuo and L. Ding, Lead-free Perovskite Materials $(NH_4)_3Sb_2I_xBr_{9-x}$, *Angew. Chem., Int. Ed.*, 2017, **56**, 6528–6532.

25 T. Okanoa and Y. Suzuki, Gas-assisted coating of Bi-based $(CH_3NH_3)_3Bi_2I_9$ active layer in perovskite solar cells, *Mater. Lett.*, 2017, **191**, 77–79.

26 K. Ahmad, S. N. Ansari, K. Natarajan and S. M. Mobin, A $(CH_3NH_3)_3Bi_2I_9$ Perovskite Based on a Two-Step Deposition Method: Lead-Free, Highly Stable, and with Enhanced Photovoltaic Performance, *ChemElectroChem*, 2019, **6**, 1192–1198.

27 A. Kulkarni, T. Singh, M. Ikegami and T. Miyasaka, Photovoltaic enhancement of bismuth halide hybrid perovskite by N-methyl pyrrolidone-assisted morphology conversion, *RSC Adv.*, 2017, **7**, 9456–9460.

28 J. Huang, Z. Gu, X. Zhang, G. Wu and H. Chen, Lead-free $(CH_3NH_3)_3Bi_2I_9$ perovskite solar cells with fluorinated PDI films as organic electron transport layer, *J. Alloys Compd.*, 2018, **767**, 870–876.

29 S. Sun, S. Tominaka, J.-H. Lee, F. Xie, P. D. Bristowe and A. K. Cheetham, Synthesis, crystal structure, and properties of a perovskite-related bismuth phase, $(NH_4)_3Bi_2I_9$, *APL Mater.*, 2016, **4**, 031101.

30 R. Zhuang, X. Wang, W. Ma, Y. Wu, X. Chen, L. Tang, H. Zhu, J. Liu, L. Wu, W. Zhou, X. Liu and Y. Yang, Highly sensitive X-ray detector made of layered perovskite-like $(NH_4)_3Bi_2I_9$ single crystal with anisotropic response, *Nat. Photonics*, 2019, **13**, 602–608.

31 M. R. Filip, S. Hillman, A. A. Haghighirad, H. J. Snaith and F. Giustino, Band Gaps of the Lead-Free Halide Double Perovskites $Cs_2BiAgCl_6$ and $Cs_2BiAgBr_6$ from Theory and Experiment, *J. Phys. Chem. Lett.*, 2016, **7**, 2579–2585.

32 Y. Kim, Z. Yang, A. Jain, O. Voznyy, G.-H. Kim, M. Liu, L. N. Quan, F. P. Garcia de Arquer, R. Comin, J. Z. Fan and E. H. Sargent, Pure Cubic-Phase Hybrid Iodobismuthates $AgBi_2I_7$ for Thin-Film Photovoltaics, *Angew. Chem., Int. Ed.*, 2016, **55**, 9586.

33 Z. Shao, T. Le Mercier, M. B. Madec and T. Pauporte, Exploring $AgBi_xI_{3x+1}$ semiconductor thin films for lead-free perovskite solar cells, *Mater. Des.*, 2018, **141**, 81.

34 Z. Shao, T. L. Mercier, M. B. Madec and T. Pauporte, $AgBi_2I_7$ layers with controlled surface morphology for solar cells with improved charge collection, *Mater. Lett.*, 2018, **221**, 135.

35 H. Zhu, M. Pan, M. B. Johansson and E. M. J. Johansson, High photon-to-current conversion in solar cells based on light-absorbing silver bismuth iodide, *ChemSusChem*, 2017, **10**, 2592–2596.

36 C. C. Stoumpos and K. G. Mercouri, The renaissance of halide perovskites and their evolution as emerging semiconductors, *Acc. Chem. Res.*, 2015, **48**, 2791–2802.

37 Z. Tang, T. Bessho, F. Awai, T. Kinoshita, M. M. Maitani, R. Jono, T. N. Murakami, H. Wang, T. Kubo, S. Uchida and H. Segawa, Hysteresis-free perovskite solar cells made of potassium-doped organometal halide perovskite, *Sci. Rep.*, 2017, **7**, 12183.

38 X. Chen, Y. Myung, A. Thind, Z. Gao, B. Yin, M. Shen, S. Beom Cho, P. Cheng, B. Sadtler, R. Mishra and P. Banerjee, Atmospheric pressure chemical vapor deposition of methylammonium bismuth iodide thin films, *J. Mater. Chem. A*, 2017, **5**, 24728–24739.

39 X. Qiu, Y. Jiang, H. Zhang, Z. Qiu, S. Yuan, P. Wang and B. Cao, Lead-free mesoscopic Cs_2SnI_6 perovskite solar cells using different nanostructured ZnO nanorods as electron transport layers, *Phys. Status Solidi RRL*, 2016, **10**, 587–591.

40 Z. Shao, T. Le Mercier, M. B. Madec and T. Pauporté, $AgBi_2I_7$ layers with controlled surface morphology for solar cells with improved charge collection, *Mater. Lett.*, 2018, **221**, 135–138.

41 S. Chatterjee and A. J. Pal, Tin(IV) Substitution in $(CH_3NH_3)_3Sb_2I_9$: Toward Low-Band-Gap Defect-Ordered Hybrid Perovskite Solar Cells, *ACS Appl. Mater. Interfaces*, 2018, **10**, 35194–35205.

42 C. Zhang, L. Gao, S. Teo, Z. Guo, Z. Xu, S. Zhao and T. Ma, Design of a novel and highly stable lead-free Cs_2NaBiI_6 double perovskite for photovoltaic application, *Sustainable Energy Fuels*, 2018, **2**, 2419–2428.

43 M. B. Johansson, B. Philippe, A. Banerjee, D. Phuyal, S. Mukherjee, S. Chakraborty, M. Cameau, H. Zhu, R. Ahuja, G. Boschloo, H. Rensmo and E. M. J. Johansson, Cesium Bismuth Iodide Solar Cells from Systematic Molar Ratio Variation of CsI and BiI3, *Inorg. Chem.*, 2019, **58**, 12040–12052.

44 C. Zuo and L. Ding, Lead-free Perovskite Materials $(NH_4)_3Sb_2I_xBr_{9-x}$, *Angew. Chem.*, 2017, **129**, 6628–6632.

45 T. Yokoyama, T. B. Song, D. H. Cao, C. C. Stoumpos, S. Aramaki and M. G. Kanatzidis, The Origin of Lower Hole Carrier Concentration in Methylammonium Tin Halide Films Grown by a Vapor-Assisted Solution Process, *ACS Energy Lett.*, 2017, **2**, 22–28.

46 K. Ahmad, P. Kumar, P. Shrivastava and S. M. Mobin, Sn(IV) Inserted Lead-Free Perovskite Materials $(MA_3(Bi_{1-x}Sn_x)_2I_9)$ as Light Absorbers: Bandgap Engineering and Enhanced Photovoltaic Performance, *Energy Technol.*, 2022, **10**, 2100717.

47 M. Burgelman, P. Nollet and S. Degrave, Modelling polycrystalline semiconductor solar cells, *Thin Solid Films*, 2000, **361**, 527–532.